Tectonic geomorphology of the Ash Hill fault, Panamint Valley, California

Alexander L. Densmore and Robert S. Anderson

Institute of Tectonics and Department of Earth Sciences,
University of California, Santa Cruz, CA 95064, USA (email:
adens@earthsci.ucsc.edu)

ABSTRACT

Panamint Valley, in eastern California, is an extensional basin currently bounded by active, dextral-normal oblique-slip faults. There is considerable debate over the tectonic and topographic evolution of the valley. The least-studied structure, the Ash Hill fault, runs for some 50 km along the valley's western edge, and active strands of the fault continue south into the neighbouring Slate Range. Vertical displacement on the fault is valley-side up, creating topography that conflicts with the gross morphology of the valley itself. We use this topography, along with kinematic and geological markers, to constrain the Quaternary slip rate and orientation of the Ash Hill fault. The fault offsets all but the active channel deposits in the valley, and slickenlines indicate a strike-slip to dip-slip ratio of 3.5:1. An offset volcanic unit dated at 4 Ma provides a minimum slip rate of 0.3 ± 0.1 mm yr^{-1}, and a long-term strike-slip to dip-slip ratio of 5.2:1. Slip on the fault has warped a palaeolake shoreline within the valley. Simple elastic dislocation modelling of the vertical deformation of the shoreline suggests total fault slip of ≈ 60 m, valley-side up. The shoreline probably dates to 120–150 ka, implying a late Quaternary slip rate of 0.4–0.5 mm yr^{-1}. We suggest two possible mechanisms for the apparently anomalous slip behaviour of the Ash Hill fault. The fault may be a listric structure related to the proposed low-angle fault underlying Panamint Valley. Alternatively, the Ash Hill fault is a high-angle fault, implying that the valley is currently bounded by high-angle dextral-slip faults. Lack of detailed subsurface information precludes any knowledge of the true relationships between the presently active faults.

INTRODUCTION

Panamint Valley is a 100-km-long trough in eastern California, near the western edge of the extensional Great Basin (Fig. 1). The valley is elongate and deep, with nearly 3000 m of relief between the basin floor and the crest of the Panamint Range (Fig. 1). A broad arch divides the valley into two sub-basins, each currently occupied by a playa (Smith, 1976).

Panamint Valley lies within a NW-trending zone of right-lateral and normal faulting (e.g. Wright, 1976), and active faults have long been recognized within Panamint Valley itself (Hopper, 1947; Hall, 1971; Smith, 1976). We focus here on one of these structures, the Ash Hill fault, which parallels the western edge of the valley for some 50 km (Fig. 2). The fault is of interest for several reasons. First, it has received relatively little attention from previous workers; Smith (1976) constructed a reconnaissance map of the fault, while the quadrangle map of Hall (1971) includes the fault's northern tip. The southern continuation of the fault, near the crest of the Slate Range (Fig. 2), was mapped by Smith *et al.* (1968).

Second, the Ash Hill fault is in close proximity to the dominant structure within the valley, the Panamint Valley fault zone. This fault zone bounds the entire eastern edge of the valley, changing strike to merge with the Hunter Mountain fault at the valley's extreme northern end (Fig. 1). The zone itself consists of multiple strands with highly variable slip orientations. Several low-angle normal faults are exposed in the Panamint Range, both at and east of the range front (Hodges *et al.,* 1989). The most westerly of these faults is still active (Hodges *et al.,* 1989). Just west of the range front are a series of high-angle, dextral-slip faults that form scarps in Quaternary alluvium (Hopper, 1947; Smith, 1976; Hodges *et al.,* 1989; Zhang *et al.,* 1990; Cichanski, 1993; Densmore & Anderson, 1994). This apparent partitioning of active slip into normal and dextral components has led to two hypotheses about the relative importance of the active high-angle dip-slip structures within the valley.

The first hypothesis holds that the modern valley opened by normal slip on a Panamint Valley fault zone that dips 0–15°W (Burchfiel *et al.,* 1987; Hodges *et al.,*
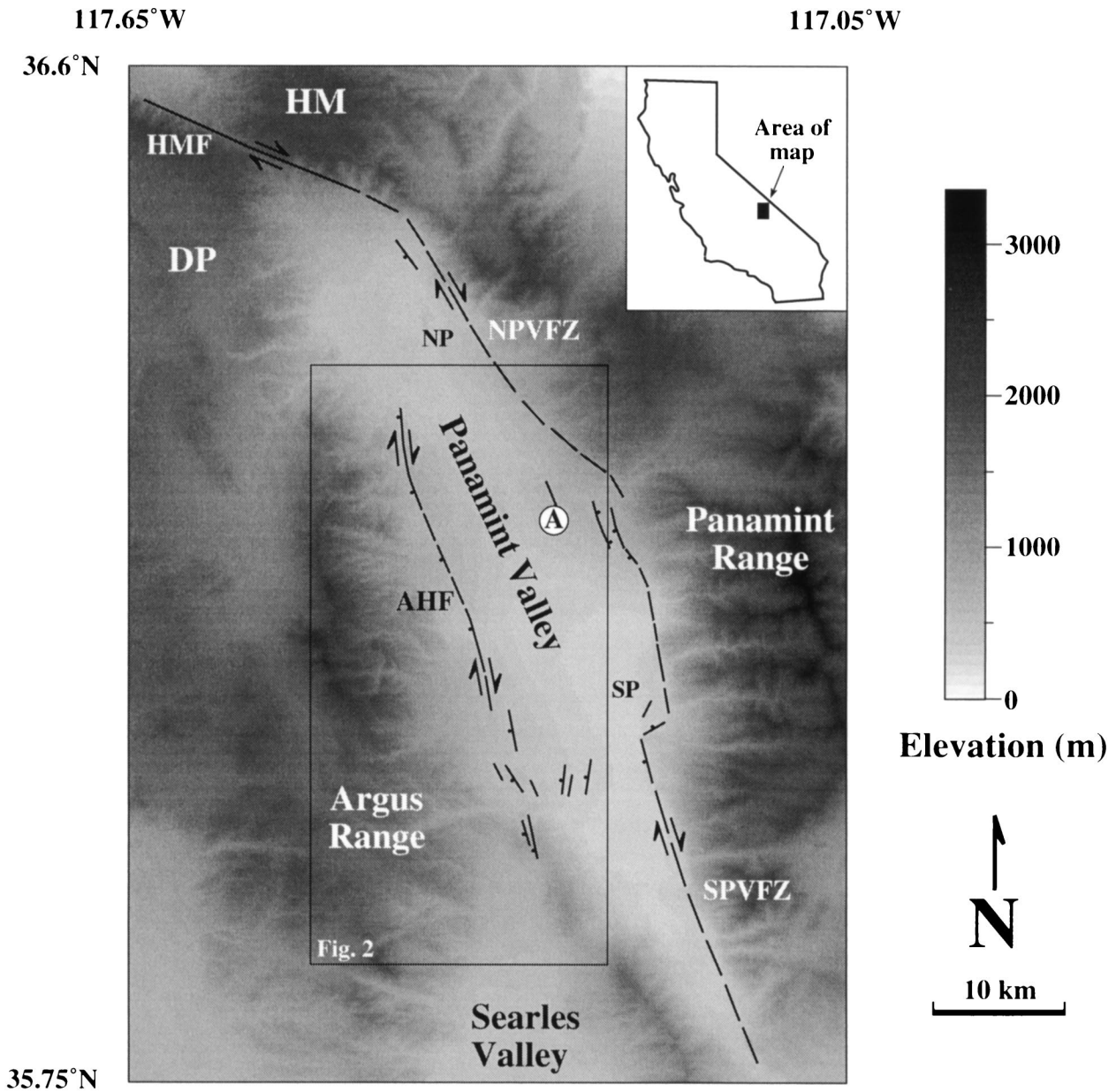
Fig. 1. Map of Panamint Valley and surrounding region. Topography is from USGS DEM data, with 3 arc-second resolution. Darker pixels represent higher elevations. Active faults within the valley are shown; relative strike-slip motion is shown by arrows, while dip-slip motion is denoted by a ball on the downthrown block. HM, Hunter Mountain; DP, Darwin Plateau; AHF, Ash Hill fault; HMF, Hunter Mountain fault; NPVFZ, north Panamint Valley fault zone; SPVFZ, south Panamint Valley fault zone; NP, north Panamint playa; SP, south Panamint playa. The circled 'A' marks the mid-valley arch that separates the north and south playas. The area enclosed by the box is shown in Fig. 2.

1989). This hypothesis is supported by the shallow (≈ 100 m) depth to basement in the northern valley, as determined by well logs and geophysical surveying (Smith & Pratt, 1957; MIT & Biehler, 1987). Hodges *et al.* (1989) documented several abandoned low-angle normal faults east of the modern valley, and proposed that the modern Panamint Valley is the latest and most westerly in a series of depocentres primarily controlled by low-angle normal faulting. The extension is parallel to the trace of the dextral-slip Hunter Mountain fault, which strikes N60°W (Fig. 1). This extension direction is not normal to the surface trace of the Panamint Valley fault

zone, resulting in a component of dextral slip that is accommodated by upper-plate or otherwise minor high-angle faults (Hodges *et al.*, 1989).

The second hypothesis argues that, while the Panamint Valley fault zone may have been dominantly normal-slip in the past, the presently active strand is a deep-seated, high-angle dextral-slip fault (Ellis, 1993; Ellis *et al.*, 1995). The shallow depth to basement in the northern end of the valley may then be explained by uplift within the restraining bend formed by the Panamint Valley and Hunter Mountain faults (Ellis, 1993; Ellis *et al.*, 1995). Ellis *et al.* (1995) calculated the surficial displacement
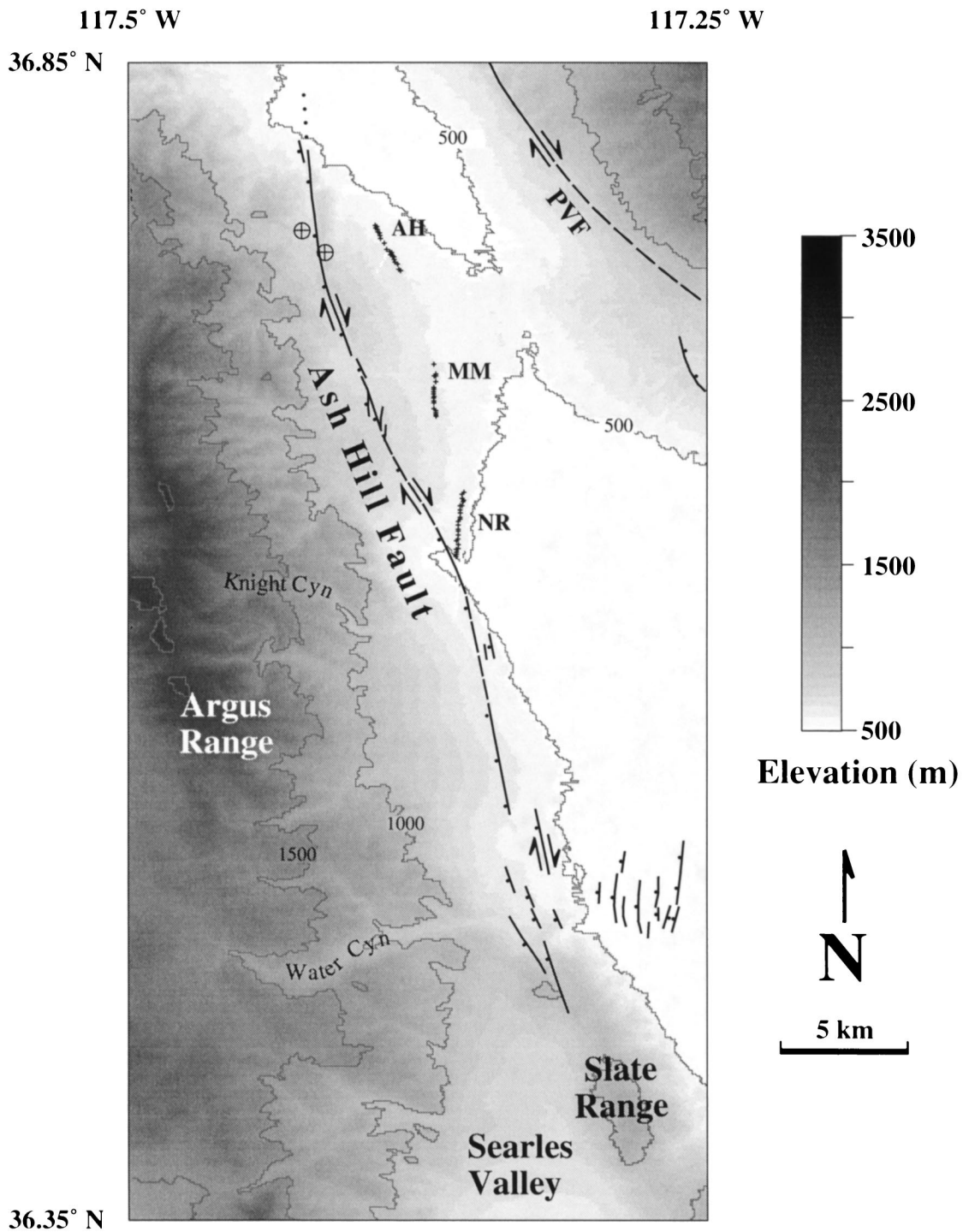
117.5° W   117.25° W

36.85° N

36.35° N

Fig. 2. Strip map of the Ash Hill fault in Panamint Valley. Topography is from USGS DEM data, with 3 arc-second resolution. Darker pixels represent higher elevations. Contour interval is 500 m. Active strands of the Ash Hill and Panamint Valley faults are shown; relative strike-slip motion is shown by arrows, while relative dip-slip motion is denoted by a ball on the downthrown block. The circled crosses mark the southernmost outcrop of basalt on Ash Hill and the Argus Range, used as a piercing line across the Ash Hill fault. The small crosses are surveyed points along segments of a deformed palaeoshoreline of Lake Panamint; AH, Ash Hill segment; MM, Minietta Mine segment; NR, Nadeau Road segment.

field associated with the observed fault geometry, and were able to reproduce qualitatively the present valley floor topography using a far-field extension direction of N70°W.

Available stress data in the region are consistent with both dextral and normal fault slip. Schweig (1989) used fault kinematic data from the nearby Darwin Plateau to determine principal stress orientations. He found the present-day S_3 to be orientated N87 °W, while S_2 is orientated approximately N-S and S_1 is near-vertical.

Schweig (1989) also concluded that $S_2 \sim S_1$, and noticed a change from ENE-directed extension to the present WNW-directed extension sometime after 5.7 Ma. Zoback (1989) employed data from the 1872 Owens Valley earthquake to infer a similar modern stress state, with S_3 orientated N80–85°W and $S_2 \sim S_1$. Wright (1976) and Ellis (1993) reached similar conclusions using a variety of geological and earthquake data.

It seems clear that a combination of dextral and normal slip produced the modern Panamint Valley; the differences between the two hypotheses outlined above lie in the relative magnitudes of those two components, in the subsurface geometry of the Panamint Valley fault zone, and in the temporal history of slip orientation. Resolution of these differences is beyond the scope of this paper. However, we introduce the hypotheses in order to motivate our work on the neighbouring Ash Hill fault. We document both the slip rate and orientation of the Ash Hill fault through time. This information will place constraints on both the active tectonic regime within the valley and on how that regime has evolved. Any model of the Panamint Valley fault zone, and thus of valley evolution, must be consistent with those constraints.

The goals of this study are three-fold: (i) to determine the slip direction and rate of the Ash Hill fault from geomorphology and slickenlines; (ii) to document deformation of palaeohorizontal markers (shorelines) near the fault; and (iii) to derive constraints on the behaviour of the fault by applying numerical models of fault displacements to those markers.

FIELD RELATIONS

Fault geology and geomorphology

We mapped segments of the Ash Hill fault at a scale of 1:24 000. At its southernmost exposure, the fault forms a series of small playas or sag ponds in the crest of the northern Slate Range (Fig. 2). At least two active, steeply west-dipping strands may be traced for several kilometres from the Slate Range crest down onto the floor of Panamint Valley. The western strand forms a low (≈ 1 m), west-facing scarp in all but the most recent stream gravel. Toward the north, slip seems to shift progressively from the eastern to the western strands. Just north of the Slate Range, the strands splinter into a complex zone of faulting. A number of short, west-dipping fault segments form west-facing scarps, producing a set of hills up to 30 m high on the valley floor (Fig. 2). In this area, the Ash Hill fault and the Panamint Valley fault zone are separated by less than 10 km; this shattered zone is possibly due to interaction and slip partitioning between these faults.

North of Water Canyon, the Ash Hill fault coalesces into a single strand that is traceable for 30 km (Fig. 2). The fault is exposed as a low (2–5 m), west-facing scarp in the bajada of the Argus Range. Uplifted fans east of the fault have gradients of up to 6°, in contrast to fan

gradients west of the fault of 3–4°. Uplift has also isolated and protected sections of the fans from active deposition, allowing extensive desert pavements to develop and enabling individual clasts to acquire a thick coat of desert varnish. In the centre of the valley, just north of Knight Canyon, the scarp abruptly grows to 20–30 m in height (Fig. 2). This change in scarp height is in part due to southward translation of a large fan complex, probably derived from the large drainages in the northern Argus Range. The change in height may also be due to the $\approx 10°$ change in strike of the Ash Hill fault at this point, which forms a restraining bend. The fanglomerate exposed in the scarp is folded into a broad NW-trending warp, which we interpret as a feature of the near-fault deformation field. The fault plane itself is expressed as a thick (up to 1.0 m), steeply ($> 75°$) west-dipping sheet or vein of calcite, with entrained alluvial clasts and breccia fragments (Fig. 3). Slickenlines are exposed both on this main sheet and on secondary veins associated with minor faults. A 0.2–0.4-m free face is exposed for ≈ 1.5 km, suggesting Holocene activity. Offset gullies, shutter ridges and small obliquely orientated graben along
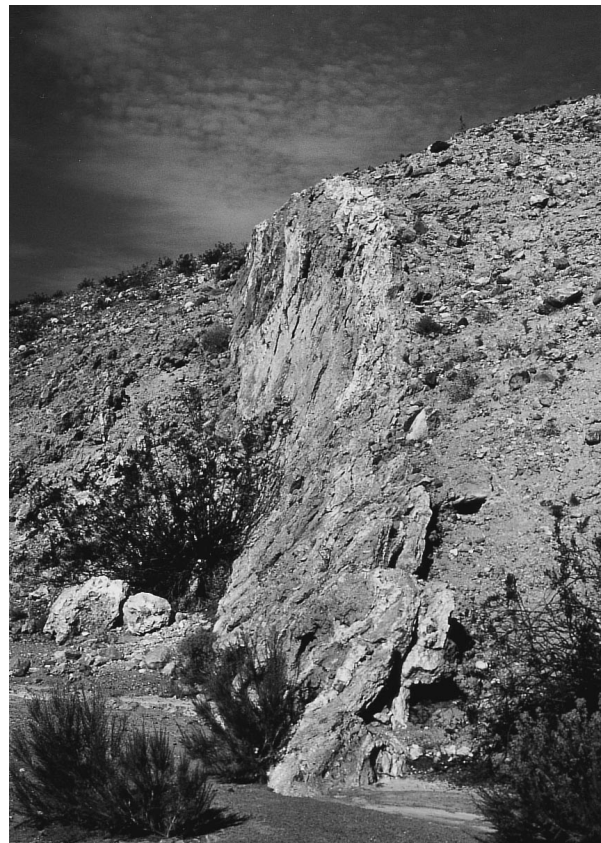

Fig. 3. Photograph of the Ash Hill fault plane near the mouth of Knight Canyon. View is to the north-west. The small bushes in the left foreground are ≈ 1.0 m high. The fault is expressed as a 0.75–1.0-m-thick sheet of calcite fault rock, with entrained alluvial clasts and breccia. Slickenlines are preserved as tool marks on the entrained clasts. The block on the right has moved up and south relative to the block on the left, creating a dextral-normal sense of slip.

the fault trace indicate a significant component of dextral slip. Gully offsets range from 2 to 60 m.

The scarp remains at least 10 m high to the north, forming Ash Hill itself. The fault strike rotates clockwise from N35°W to N2°W (Fig. 2). A basalt unit capping Ash Hill is offset in a dextral-normal sense across the fault, and the large channels cutting Ash Hill appear to be offset from their sources. A 0.5–1.0-m scarp persists in all but the active stream gravel. At its northern end, the fault disappears beneath a large alluvial fan deposit associated with Darwin Canyon.

Kinematic indicators and long-term slip rate

We collected slickenline orientations from nine locations along the fault (Fig. 4). Most of the slickenlines were fresh-looking tool marks inscribed on cobbles within the calcite fault rock. We are less confident of the few isolated locations where we collected slickenlines from uncemented clasts. Slickenlines from the central part of the fault show a slip vector orientated 321°, 16°, and a strike-slip to dip-slip ratio of 3.5:1. Those lines from minor, north-striking faults are much more steeply dipping, consistent with normal, *en echelon* faulting within a dextral-slip zone.

We have not inverted our kinematic data for stress directions, owing to the often unreasonable assumptions that must be made in such analyses (Pollard *et al.*, 1993). However, we note that our data are consistent with the stress directions presented by Schweig (1989) and Zoback (1989). Specifically, the apparent coexistence of dextral

and normal slip, and the observation that slip becomes more normal as fault strike is rotated from north-west to north, indicate a WNW orientation for S_3. The dextral-normal coexistence also strengthens the argument that S_2 and S_1 are similar in magnitude and may switch in orientation.

Offset of the basaltic unit that caps Ash Hill itself constrains both the total amount of slip and a maximum slip rate on the Ash Hill fault. The southern edge of the unit has been dextrally offset 1200 ± 300 m horizontally by the fault, as mapped by Hall (1971) (Fig. 5); the unit is not exposed close to the fault, precluding a better offset estimate. While the base of the basalt is poorly exposed, the vertical offset of the unit may be obtained from its upper surface. This low-relief surface is well-exposed and fairly continuous on the Argus Range west of the fault, and appears to be a primary flow surface (Fig. 5). The low-relief top of Ash Hill, east of the fault, appears to represent the same surface; the two are morphologically similar, and basalts from east and west of the fault look alike in hand sample. The surfaces are vertically offset 230 ± 30 m across the Ash Hill fault. The total offset is thus 1220 ± 300 m, and the strike-slip to dip-slip ratio is 5.2:1, similar to the late Quaternary slip orientation of 3.5:1 cited above. Hall (1971) reports a K/Ar date from an olivine basalt sample taken from northern Ash Hill of 4.05 ± 0.15 Ma. When combined with our total measured offset of 1220 ± 300 m, this age yields a minimum, long-term slip rate of 0.3 ± 0.1 mm yr^{-1}.

Palaeoshoreline survey

Measurement of the deformation of palaeohorizontal lines is a powerful tool for quantifying fault slip (e.g. Smith, 1976; Valensise & Ward, 1991; Anderson & Menking, 1994). We applied the technique to a prominent shoreline that crops out discontinuously for 15 km near the Ash Hill fault (Figs 2 and 6). The shoreline formed during a high stand of Lake Panamint, one of the Owens River system of pluvial lakes, and is expressed here as a cut bench, 5–10 m wide. The bench is covered with sub-rounded to subangular gravel, forming excellent desert pavements (Smith, 1976). Below this bench is a band of lithoid tufa that occurs as large (up to 1 m) heads, commonly as rinds around boulders or cobbles (Smith, 1976). The bench is often backed by a low cliff, which we interpret to be wave-cut. Smith (1976) noted that the shoreline is offset 27 ± 5 m, down to the west, across the Ash Hill fault, although we were unable to locate his correlative shoreline exposure west of the fault.

The age of the shoreline is not known, as no radiometric date on the shoreline sediments is available (Fitzpatrick & Bischoff, 1993). Smith (1976) correlated the shoreline with his Gale-Stage lake high stand, the height of which was controlled by the elevation of the sill or spill point of Panamint Valley. Maintenance of the water surface at this high stand elevation required a
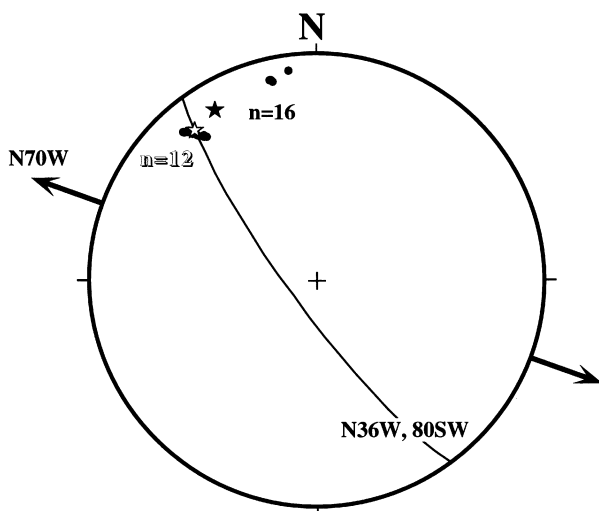

Fig. 4. Lower-hemisphere, equal-area projection of slip vectors from the Ash Hill fault. The mean vector ($n = 16$) is orientated 329°,14°, and is plotted as a black star. The mean vector of a subset ($n = 12$) of the highest-quality data is orientated 321°,16°, and is plotted as a white star. The heavy arrows show the N70°W extension direction predicted by numerical modelling (Ellis, 1993; Ellis *et al.*, 1995); this is similar to the S_3 directions calculated by Schweig (1989) and Zoback (1989). Also shown is the attitude of the fault plane as measured at the surface near the Nadeau Road shoreline segment.

Fig. 5. Oblique aerial photograph of Ash Hill and the northern Ash Hill fault. View is to the north, along the surface trace of the fault, from an altitude of ≈ 200 m. Ash Hill is the dark, basalt-capped hill on the right side of the photo. The fault, here concealed by alluvium, runs straight up the centre of the image, along the western edge of Ash Hill. The basalt in the left middle distance, west of the fault, lies on the flanks of the Argus Range, and is the southernmost exposure of basalt for several tens of kilometres. Dextral motion along the fault has offset the southern edge of the basalt 1200 ± 300 m (to the middle foreground). The smooth upper surface of the flow has been vertically offset 230 ± 30 m, giving a total offset of 1220 ± 300 m. The north Panamint playa is visible as the tan patch in the right middle distance.

Fig. 6. Oblique aerial photograph of the Nadeau Road shoreline segment. View is to the north-west from an altitude of ≈ 150 m. Most of the field of view is the uplifted footwall of the Ash Hill fault; it is incised by ephemeral streams, and dark desert pavements have developed on the interfluves. The lighter band trending from lower-left to upper-right is a field of lithoid tufa, 5–15 m wide. Just upslope from the tufa band is a series of darker blotches; these are outcrops of subrounded to subangular, varnished beach gravel, formed into well-developed desert pavement. The Ash Hill fault runs diagonally across the upper-left corner, and separates modern, active fan deposits (extreme upper-left) from older, uplifted, incised fan remnants. The north Panamint playa is visible as the lighter patch in the upper-right corner.

consistent influx of water to overcome evaporative losses. Since the drainage area directly feeding Panamint Valley is relatively small, Smith (1976) concluded that high stands of Lake Panamint occurred during periods of spill from Searles Lake, the next upstream lake in the Owens River chain. The Searles Lake depth chronology has been well constrained through the use of radiometric dating techniques (e.g. Jannik *et al.,* 1991; Bischoff *et al.,* 1985). Jannik *et al.* (1991) found evidence for spill between Searles and Panamint valleys at 120–150 ka and at 10–24 ka. The observed amount of fluvial incision into the shoreline probably rules out the younger interval, leaving 120–150 ka as the most likely age range.

We surveyed profiles along three segments of the shoreline, each between 1.0 and 2.5 km long, using a total station EDM. From south to north, we refer to the segments as the Nadeau Road, Minietta Mine and Ash Hill shorelines (Fig. 2). Our chosen survey horizon was the uppermost exposure of large, in-place tufa blocks or rinds; this represents a distinctive, easily traceable horizon in the field (Fig. 6), and the presence of tufa rinds around the bases of boulders implies little reworking of the shoreline deposit. We note that tufa may form at a range of depths within a lake (Benson, 1994), and that the uppermost exposure of tufa may not therefore represent a palaeohorizontal surface. However, the coexistence of the tufa line with the cliff and bench morphology implies

that the chosen horizon is very close to the palaeolake surface. Changes in elevation between repeated shots to the same mark were ≤ 2.5 cm. Thus, the primary source of error in the data comes from the accuracy with which the survey horizon may be 'picked'. Errors in visually picking the horizon are estimated to be ± 0.5 m in the vertical; the low gradient of the surface in the cross-strike direction ($\approx 2°$) implies that even large discrepancies in the horizontal position result in small elevation errors.

We found that all three surveyed segments of this once-horizontal shoreline are now tilted or warped, so that they slope down to the north-east across strike, and down to the north-west along strike (Fig. 7). The highest magnitude of warping is in the across-strike or fault-normal direction. This is consistent with the deformation pattern produced by dip slip on a dipping, planar fault, which should vary most in the fault-normal direction. In particular, the Nadeau Road segment has experienced differential vertical motion of ≈ 3.5 m over a fault-normal distance of 2000 m (Fig. 7a). The Minietta Mine

and Ash Hill segments, being further from the surface trace of the Ash Hill fault, are less deformed.

We hypothesized that the primary cause of this deformation was slip on the Ash Hill fault. Since we could not locate a site where the fault offsets the shoreline, we could not directly measure the amount of fault slip since shoreline formation. We therefore turned to numerical models of the deformation field produced by the Ash Hill fault, and attempted to match that deformation field to our measured shoreline profiles.

NUMERICAL MODELLING

We applied a simple, 3-D elastic half-space dislocation model (Mansinha & Smylie, 1971) to the surveyed shoreline profiles. By systematically varying fault orientation and slip, we found the surficial vertical displacement field that most closely mimics the uplift recorded in the shoreline profile. The rake was fixed at 164°, as measured from slickenlines in the field. We swept through a range of values for fault dip, total slip, and top and base of the rupture plane (Table 1). Goodness of fit was assessed by minimizing χ^2 and maximizing variance reduction.

Nadeau Road shoreline segment

The best-fit Nadeau Road model predicts ≈ 60 m of total relative slip on a shallow (0.2–1.5 km deep), 80°W-dipping fault since the abandonment of the shoreline (Fig. 8, Table 1). This model explains 98.8% of the variance in the data set, and has a χ^2 of 13.3. Since the rake is 164°, the amount of predicted dip-slip is (60 m)* sin(164°), or 17 m. This is slightly less than the 27 ± 5 m vertical offset of the shoreline reported across the Ash Hill fault (Smith, 1976). If the shoreline formed during the 120–150 ka spill interval, as noted above, then the ≈ 60 m of slip yields a minimum late Quaternary slip rate on the Ash Hill fault of 0.4–0.5 mm yr^{-1}.

It is instructive to compare this modelled slip with the longer term slip orientation and rate derived from the offset basalt. The minimum slip rates recorded in both the basalt and the shoreline differ by at most a factor of 2–3, and the ratios of strike-slip to dip-slip are very similar. It thus appears that the slip behaviour of the Ash Hill fault has been relatively consistent over most of the Quaternary.

Surveyed profiles, all shoreline segments
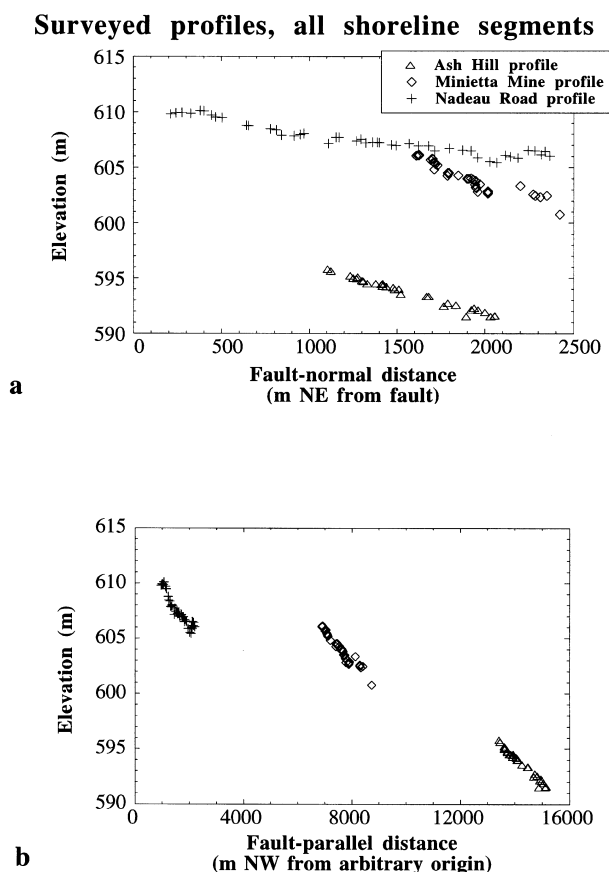

a

b

Fig. 7. Surveyed profiles of all three shoreline segments. (a) Surveyed profiles projected along a line perpendicular to the Ash Hill fault. Distance increases to the north-east, away from the fault. Note that all three segments are tilted down to the north-east. (b) Surveyed profiles projected along a line parallel to the Ash Hill fault. Distance increases to the north-west, away from an arbitrary origin. All three segments are tilted down to the north-west.

Table 1. Model parameter search results.

	Slip (m)	Dip	Depth to top (km)	Depth to base (km)
Search range	2–100	30°W–90°W	0–5.0	1.0–10.0
Increment	2	2°	0.1	0.1
Best fit	60	80°	0.2	1.5

**Nadeau Road shoreline profile
and DISLOC model fit**

chi² 13.3
variance reduction 98.8%
slip 60 m
dip 80°
rake 164°
top of fault plane 0.2 km
base of fault plane 1.5 km
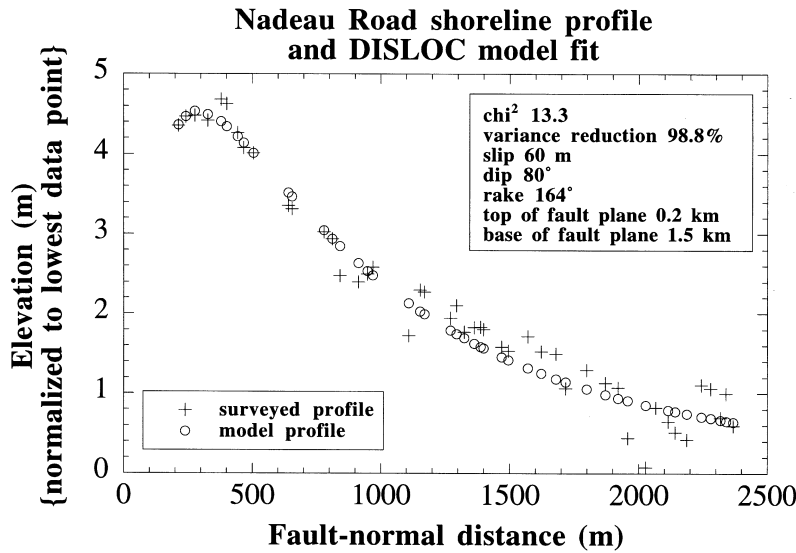
+ **surveyed profile**
○ **model profile**

Fig. 8. Fault-normal surveyed elevation profile of the Nadeau Road shoreline (crosses) and best-fitting numerical model results (circles). Fault strike and rake were fixed at field-determined values.

The model results are extremely sensitive to changes in the depths of the top and base of the fault plane (Fig. 9). The depth to the top of the fault is well-constrained by the slight rollover, or decrease in vertical displacement, shown by the three surveyed data points closest to the fault (Fig. 8). If the fault is allowed to
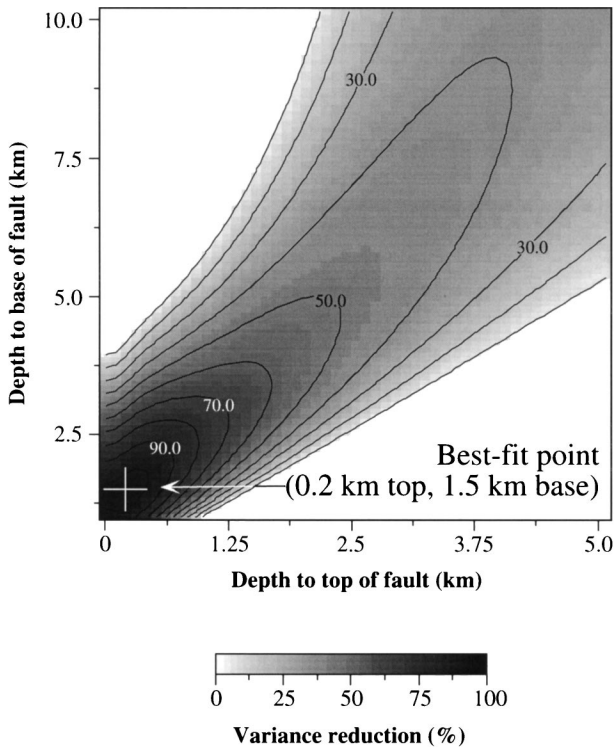

Fig. 9. Error surface for the model runs on the Nadeau Road data set, as a function of depth to the top and depth to the base of the model fault plane. Error is expressed as variance reduction, in per cent. Contour interval is 10%. High values mean that much of the variance in the data is explained by the model, and thus indicate a good fit to the data. The white cross shows the best-fitting fault plane, which extends from 0.2 to 1.5 km depth. That particular model explains 98.8% of the variance in the original data.

rupture to the surface, then vertical displacement increases monotonically as the fault is approached. The presence of the rollover constrains the top of the fault to a depth of 0.2–0.3 km. Likewise, the rapid decrease in shoreline vertical displacement with distance from the fault (Fig. 8) limits the depth to the fault base; a depth greater than 1.5 km results in model displacements that are unacceptably high at points far from the fault (e.g. King *et al.*, 1988).

This somewhat shallow fault depth is very close to the 2–4 km effective elastic thickness inferred for the western United States (e.g. King *et al.*, 1988; Stein *et al.*, 1988; King & Ellis, 1990). Those studies used a two-layer numerical model with both elastic and viscous rheologies. Stein *et al.* (1988) compared model fault profiles to field examples of dip-slip faults, and found that geological structures could be accurately reproduced by coseismic slip on a 2–4-km-thick elastic layer, coupled with inter-seismic slip on an underlying, relaxing viscous half-space.

Minietta Mine and Ash Hill segments

We hoped to verify our Nadeau Road results by modelling the deformation patterns of the Minietta Mine and Ash Hill segments. However, we were unable to reproduce these shoreline profiles adequately with the elastic half-space model. On both segments, deformation decreases very rapidly with distance from the fault. As detailed above, this high degree of curvature requires an unreasonably shallow model fault plane.

We propose several reasons for our failure to match the deformation profiles. We note that both the Minietta Mine and Ash Hill segments are at least 2 km from the surface trace of the Ash Hill fault (Fig. 2). The calculated uplift at such distances is ≤ 1 m (Fig. 8), at or near the level of our survey error. It is therefore probable that any signal recorded by these segments is below our level of detection. In contrast, the Nadeau Road segment approaches to within 200 m of the Ash Hill fault (Fig. 7a),

making it a much more robust recorder of displacements on the Ash Hill fault.

An alternative explanation is that the shoreline profiles have been deformed by isostatic, as well as tectonic, displacements. Isostatic deformation of shorelines following drainage of a large lake is well documented (e.g. Gilbert, 1890; Bills & May, 1987). Lake Panamint had an area of 780 km^2 and a maximum depth of 292 m at its high stand (K. Menking , personal communication, 1995), large enough to represent a significant load on the lithosphere. Smith (1976) estimated the amount of differential isostatic rebound caused by draining of his Gale-Stage high stand to be 2–3 m across the width of the valley. We have not performed a quantitative calculation of the effect of rebound on our shoreline profiles, but we note that it may well compete with or drown out the tectonic signal imposed by the Ash Hill fault, especially far from the fault where that signal is small.

A final possible explanation for the poor match between calculated and surveyed profiles is the simplicity of our model fault geometry. The above models considered slip on a single structure, the Ash Hill fault. However, the Panamint Valley fault zone lies ≈ 10 km east of the Minietta Mine and Ash Hill shoreline segments. Its long-term slip rate is not well known; Burchfiel *et al.* (1987) inferred a rate of 2.0–3.2 mm yr^{-1} over the past 3.0 Myr, while Zhang *et al.* (1990) calculated a Holocene rate of 2.1 ± 1.0 mm yr^{-1} on a strand of the southern Panamint Valley fault zone. These rates are several times higher than that of the Ash Hill fault. We suspect that deformation associated with the Panamint Valley fault zone dominates the signal recorded in the shorelines at distances greater than several kilometres from the Ash Hill fault. In particular, both the Minietta Mine and Ash Hill segments fall on the north flank of the mid-valley arch noted by Smith (1976) (Fig. 1). Both segments should thus be tilted down to the north-west as the arch grows. On both surveyed profiles, the north-western end of each segment is indeed 4–5 m lower in elevation than the southern end (Fig. 7).

DISCUSSION

We have shown that the surface exposure of the Ash Hill fault is consistent with a high-angle structure, that the fault has a Quaternary slip rate of ≈ 0.3 mm yr^{-1}, and that dextral-normal slip on that structure accounts for deformation of both geological units and near-fault palaeohorizontal markers. We would like to knit this information into the present tectonic picture within the valley. An understanding of the relation between the Ash Hill fault and the Panamint Valley fault zone remains hampered by a lack of information about the subsurface in the valley. Without this subsurface control, we must consider both the low-angle and the high-angle hypotheses outlined in the Introduction.

Modelling of the Nadeau Road shoreline profile suggests a shallow (1.5 km) depth to the base of the Ash

Hill rupture plane, consistent with models of other faults in the region. This argues for a shallow termination of the Ash Hill fault, possibly by merging into the proposed low-angle Panamint Valley fault zone. If the Ash Hill fault dips 80°W at depth, as it does at the surface, then the base of its modelled rupture plane must lie 14.5 km west of the surface trace of the Panamint Valley fault zone (Fig. 10a). If the two faults merge at depth , this suggests a dip on the Panamint Valley fault zone of arc tan(1.5 km/14.5 km), or 6°W. By comparison, Burchfiel *et al.* (1987) obtained a dip on the Panamint Valley fault zone of 0–15°W. In this scenario, the Ash Hill fault is a listric structure that soles into the master Panamint Valley fault zone; it may in time become the dominant fault in the valley, following the trend of westward fault (and depocentre) migration proposed by Hodges *et al.* (1989). Since the inferred direction of valley extension (N60°W) is not orthogonal to the strike of the Panamint Valley fault zone (N10°W to N36°W), extension is oblique, with a dextral component. The strike-slip observed on both the Ash Hill fault and on strands of the Panamint Valley fault zone accommodates this dextral shear in the upper plate of the detachment (Fig. 10a). This scenario makes geometric sense, and agrees with the valley evolution model of Hodges *et al.* (1989).

The alternative hypothesis is that the active traces of the Ash Hill fault and the Panamint Valley fault zone are independent, high-angle, dextral-slip faults with small normal components (Fig. 10b). This model is consistent with the orientation of most recent slip on both faults, but fails to predict the gross morphology of the valley. It also fails to account for the presence of the Argus Range and Darwin Plateau, without calling on at least some significant prior period of dominantly normal slip during the valley's evolution.

These hypotheses are end-members in a debate that extends far beyond the limits of Panamint Valley. Wright (1976), among others, has outlined both the high-angle strike-slip and the low-angle dip-slip models of Basin and Range extension, each with its adherents and detractors. The relative importance of each almost certainly varies from valley to valley. Geophysical surveys within Panamint Valley, on a larger scale than MIT & Biehler (1987) attempted, would do much toward resolving the controversy.

CONCLUSIONS

The Ash Hill fault is one of two active, dextral-normal oblique-slip faults within Panamint Valley. The fault is notable for its valley-side-up sense of slip, and for its continuation out of the valley and into the Slate Range to the south. Its long-term minimum slip rate is 0.3 ± 0.1 mm yr^{-1} over the past 4 Myr, as determined from an offset basalt unit. Slip on the fault is primarily dextral, with a small component of normal displacement; the orientation of this slip vector appears to have been
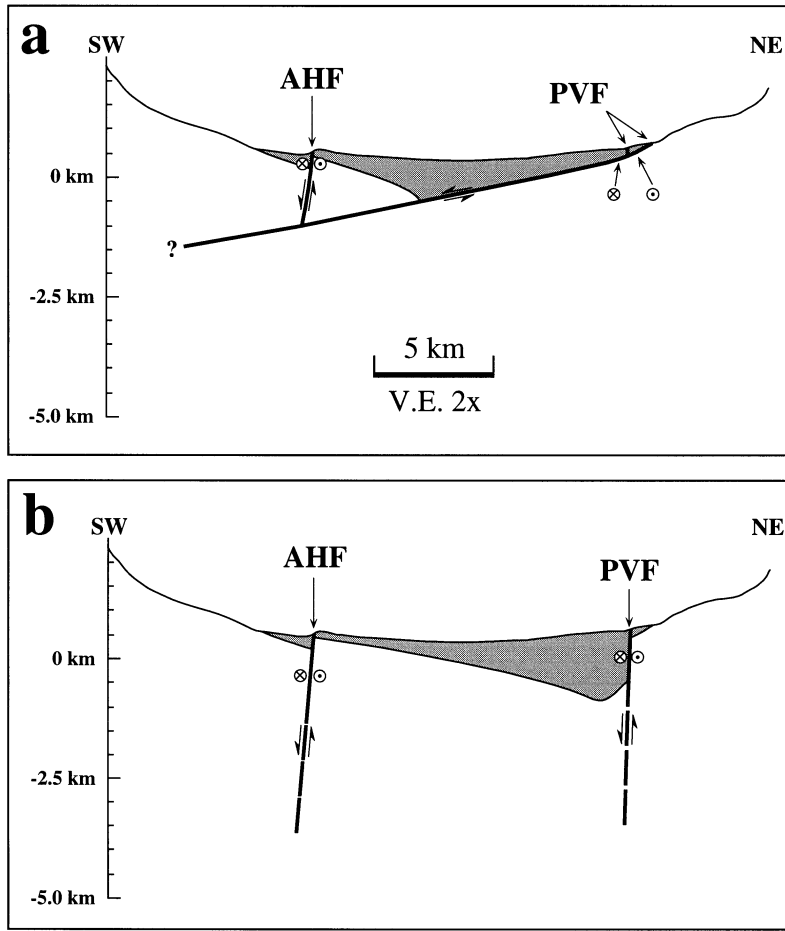
Fig. 10. Two possible cross-sections across central Panamint Valley, south of the mid-valley arch. Basement topography and thickness of basin fill are speculative. (a) Low-angle hypothesis. The Panamint Valley fault zone dips 0–15°W (Burchfiel *et al.*, 1987; Hodges *et al.*, 1989). The Ash Hill fault is a W-dipping listric fault that soles into the detachment at depth. Dextral slip is accommodated in the upper plate by a high-angle strand of the Panamint Valley fault zone. (b) High-angle hypothesis. The presently active strand of the Panamint Valley fault zone is a deep-seated dextral-slip fault. The Ash Hill fault is a steeply W-dipping, dextral-slip fault that accommodates a minor component of extension.

relatively constant over the fault's history. Motion on the Ash Hill fault has deformed a shoreline of ancient Lake Panamint, and that deformation has been modelled using numerical elastic dislocation models. Model results suggest that 60 m of slip on a shallow (1.5 km deep) fault can reproduce the observed deformation. Given a probable shoreline age of 120–150 ka, the minimum late Quaternary slip rate is 0.4–0.5 mm yr^{-1}, close to the geological rate. The Ash Hill fault may be a hangingwall splay of the Panamint Valley fault zone, or it may be an independent high-angle fault within a dextral-slip zone.

REFERENCES

ANDERSON, R.S. & MENKING, K.M. (1994) The Quaternary marine terraces of Santa Cruz, California: evidence for coseismic uplift on two faults. *Bull. Geol. Soc. Am.*, 106, 649–664.

BENSON, L.V. (1994) Carbonate deposition, Pyramid Lake subbasin, Nevada: 1. Sequence of formation and elevational distribution of carbonate deposits (Tufas). *Palaeogeog. Palaeoclim. Palaeoecol.*, 109, 55–87.

BILLS, B.G. & MAY, G.M. (1987) Lake Bonneville: constraints on lithospheric thickness and upper mantle viscosity from isostatic warping of Bonneville, Provo, and Gilbert Stage shorelines. *J. geophys. Res.*, 92, 11493–11508.

BISCHOFF, J.L., ROSENBAUER, R.J. & SMITH, G.I. (1985) Uranium-series dating of sediments from Searles Lake, California: documentation of differences between land and sea climate records. *Science*, 227, 1222–1224.

BURCHFIEL, B.C., HODGES, K.V. & ROYDEN, L.H. (1987) Geology of Panamint Valley–Saline Valley pull-apart system, California: palinspastic evidence for low-angle geometry of a Neogene range-bounding fault. *J. geophys. Res.*, 92, 10422–10426.

CICHANSKI, M.A. (1993) 'Turtleback' structure in the southwestern Panamint Mountains, Death Valley region, California. *Abstr. w. Prog. Geol. Soc. Am.*, 25, 21.

DENSMORE, A.L. & ANDERSON, R.S. (1994) Recent tectonic geomorphology of Panamint Valley, California. *EOS Supp.*, 75, 296.

ELLIS, M.A. (1993) An estimate of the recent state of stress in the Basin and Range province using topography and fault slip data. *Abstr. w. Prog. Geol. Soc. Am.*, 25, 480.

ELLIS, M.A., DENSMORE, A.L. & ANDERSON, R.S. (1995) Topography as a measure of regional strain: results of a coupled tectonic-geomorphologic model. *EOS*, 76, S279.

FITZPATRICK, J.A. & BISCHOFF, J.L. (1993) Uranium-series dates on sediments of the high shoreline of Panamint Valley, California. *Open-File Rep. U. S. Geol. Surv.*, 93-232.

GILBERT, G.K. (1890) Lake Bonneville. *Mono. U. S. Geol. Surv.*, M-0001.

HALL, W.E. (1971) Geology of the Panamint Butte quadrangle, Inyo County, California. *Bull. U.S. Geol. Surv.*, 1299.

HODGES, K.V., MCKENNA, L.W., STOCK, J., KNAPP, J., PAGE, L., STERNLOF, K., SILVERBERG, D., WÜST, G. & WALKER, J.D. (1989) Evolution of extensional basins and Basin and Range topography west of Death Valley, California. *Tectonics*, 8, 453–467.

HOPPER, R.H. (1947) Geologic section from the Sierra Nevada to Death Valley, California. *Bull. Geol. Soc. Am.*, 58, 393–432.

JANNIK, N.O., PHILLIPS, F.M., SMITH, G.I. & ELMORE, D. (1991) A ^{36}Cl chronology of lacustrine sedimentation in the Pleistocene Owens River system. *Bull. Geol. Soc. Am.*, 103, 1146–1159.

KING, G. & ELLIS, M. (1990) The origin of large local uplift in extensional regions. *Nature*, 348, 689–693.

KING, G.C.P., STEIN, R.S. & RUNDLE, J.B. (1988) The growth of geological structures by repeated earthquakes: 1. Conceptual framework. *J. geophys. Res.*, 93, 13307–13318.

MANSINHA, L. & SMYLIE, D.E. (1971) The displacement fields of inclined faults. *Bull. Seis. Soc. Am.*, 61, 1433–1440.

MIT 1985 Field Geophysics Course & BIEHLER, S. (1987) A geophysical investigation of the northern Panamint Valley, Inyo County, California: evidence for possible low-angle normal faulting at shallow depths in the crust. *J. geophys. Res.*, 92, 10427–10441.

POLLARD, D.D., SALTZER, S.D. & RUBIN, A.M. (1993) Stress inversion methods: are they based on faulty assumptions? *J. struct. Geol.*, 15, 1045–1054.

SCHWEIG, E.S. III (1989) Basin-range tectonics in the Darwin Plateau, southwestern Great Basin, California. *Bull. Geol. Soc. Am.*, 101, 652–662.

SMITH, G.I. & PRATT, W.P. (1957) Core logs from Owens, China, Searles, and Panamint basins, California. *Bull. U.S. Geol. Surv.*, 1045-A.

SMITH, G.I., TROXEL, B.W., GRAY, C.H. & VON HUENE, R. (1968) Geologic reconnaissance of the Slate Range, San Bernardino and Inyo Counties, California. *Spec. Rep. Calif. Div. Mines Geol.*, 96.

SMITH, R.S.U. (1976) *Late-Quaternary pluvial and tectonic history of Panamint Valley, Inyo and San Bernardino Counties, California.* PhD thesis, Pasadena, California Institute of Technology.

STEIN, R.S., KING, G.C.P. & RUNDLE, J.B. (1988) The growth of geological structures by repeated earthquakes: 2. Field examples of continental dip-slip faults. *J. geophys. Res.*, 93, 13319–13331.

VALENSISE, G. & WARD, S.N. (1991) Long-term uplift of the Santa Cruz coastline in response to repeated earthquakes along the San Andreas fault. *Bull. Seis. Soc. Am.*, 81, 1694–1704.

WRIGHT, L. (1976) Late Cenozoic fault patterns and stress fields in the Great Basin and westward displacement of the Sierra Nevada block. *Geology*, 4, 489–494.

ZHANG, P., ELLIS, M., SLEMMONS, D.B. & MAO, F. (1990) Right-lateral displacements and the Holocene slip rate associated with prehistoric earthquakes along the southern Panamint Valley fault zone: implications for southern Basin and Range tectonics and coastal California deformation. *J. geophys. Res.*, 95, 4857–4872.

ZOBACK, M.L. (1989) State of stress and modern deformation of the northern Basin and Range province. *J. geophys. Res.*, 94, 7105–7128.